Letter

Revealing Coulomb time shifts in high-order harmonic generation by frequency-dependent streaking

Shengjun Yue [1,2] Shan Xue,[2] Hongchuan Du [2,*] and Manfred Lein [1,†]

[1]*Leibniz University Hannover, Institute of Theoretical Physics, Appelstraße 2, 30167 Hannover, Germany*

[2]*School of Nuclear Science and Technology, Lanzhou University, Lanzhou 730000, China*

(Received 16 August 2021; revised 8 March 2022; accepted 8 April 2022; published 25 April 2022)

When an atom is ionized by a strong laser pulse, the field can drive the released electron back to the parent ion and trigger the emission of a high-order harmonic photon with a frequency that is a function of the time of ionization. The attractive Coulomb potential causes a slowdown of the outgoing electron that must be compensated by an earlier release into the accelerating field to produce the same harmonic frequency as without the Coulomb force. By numerical solution of the time-dependent Schrödinger equation for a helium model atom, we demonstrate that such a subtle time shift of about 35 attoseconds is measurable by streaking with a weak, orthogonally polarized field combined with a complex-time trajectory interpretation. A comparison of results for high and low streaking frequency shows that only the high-frequency method measures the Coulomb shift well. This is confirmed by a classical trajectory model and by the analytical R-matrix theory.

DOI: 10.1103/PhysRevA.105.L041103

The general aim of ultrafast science is the observation and control of ever faster time-dependent processes. In recent years, progress in this direction has mainly been made by means of light-based approaches. The shortest durations that have been accessed with photons are in the attosecond range and below. For example, the travel time of a high-energy photon between the two protons in hydrogen has been measured to be 247 zeptoseconds [1], the shortest light pulses created to date are around 50 attoseconds long [2,3], the relative phase between a light wave and its envelope has been controlled with 12 attoseconds precision [4], and the pulse-to-pulse delay in a pulse pair produced with polarization pulse shapers has an accuracy of 300 zeptoseconds [5].

Time measurements in attosecond physics rely heavily on *streaking methods* using the response of electrons to well-controlled moderately intense pulses. For example, the characterization of isolated attosecond light pulses, see above, uses streaking of the photoelectron that is released upon ionization by the attosecond pulse [6]. Similar methods are used for attosecond pulse trains [7,8]. In angular streaking [9–11], tunnel ionization is probed by the same field that frees the electron and the aim is to extract the electron's most probable birth time from photoelectron momentum distributions.

Furthermore, there is an analog of streaking in high-order harmonic generation (HHG). HHG denotes the process that after ionization of an atom, the laser-driven electron returns back to the initial bound state under emission of a high-frequency photon. The excursion of the electron is nearly classical and hence HHG can be modeled in terms of trajectories [12,13]. This mechanism of HHG, consisting of ionization, excursion, and recombination, is known as three-step model, and it is at the borderline of classical and quantum mechanics. Its quantum-mechanical formulation is given by the strong-field approximation (SFA) and the quantum-orbit (QO) model [14,15], where complex times are assigned to ionization and return. A streaking-type measurement of the ionization time in HHG is possible with orthogonally polarized two-color (OTC) fields [16,17]: a fundamental strong field with frequency ω is the driving field for HHG and a weak probe field with frequency 2ω polarized in the perpendicular direction serves to measure the ionization time for each generated harmonic frequency by perturbing the electron trajectory in the lateral direction. The harmonic intensity and electron return angle are measurable quantities depending on the relative phase between the two colors, facilitating the extraction of both the ionization and return times. Controlling the lateral electron dynamics by OTC fields has proven useful also for the probing and control of photoelectron emission [18–24] and for trajectory selection in HHG [25].

Streaking comes with the challenge of modeling the electron dynamics in the target system in the presence of both the external field and the electron-core Coulomb interaction. Thus, although a streaking measurement can, in principle, provide few-attosecond time resolution, the accurate retrieval of an electron birth time relies on a suitable model. In the context of HHG, the time retrieval has been based on Newtonian trajectories without the Coulomb force in the probe-field direction. Hence an important question is whether the ionization time extracted from the pioneering measurement [16] reflects the theoretically predicted Coulomb-induced time shift [26]. Intuitively speaking, this shift arises because the outgoing electron is slowed down by the Coulomb attraction (in the fundamental field direction), which must be compensated by an earlier release into the field.

In this Letter, we employ numerical solutions of the time-dependent Schrödinger equation (TDSE) to investigate the OTC scheme over a wide range of probe frequencies (with

*duhch@lzu.edu.cn

†lein@itp.uni-hannover.de

wavelengths reaching from 160 nm to 1600 nm). We find that high frequencies are superior in the sense that the true Coulomb-modified ionization time can be extracted by means of a straightforward analysis that does not require the explicit treatment of Coulomb forces in the retrieval method. By contrast, in the original ω–2ω scheme with 400 nm probe wavelength [16,17], the Coulomb shift is essentially invisible. Our conclusions are corroborated by comparison of various different classical and quantum-mechanical models.

We solve the TDSE for a two-dimensional single-active electron helium model atom, using the Crank-Nicolson method [27,28] with a time step of 0.05 a.u. on a box with size 260×100 a.u. and 2600×1000 grid points. The Hamiltonian reads (Hartree atomic units are used unless otherwise stated)

$$\hat{H} = -\tfrac{1}{2}\nabla^2 + V(\mathbf{r}) + \mathbf{r}\cdot\mathbf{E}(t). \tag{1}$$

The soft-core potential $V(\mathbf{r}) = -1/\sqrt{\mathbf{r}^2 + 0.0684}$ reproduces the ionization potential $I_p = 0.904$ a.u. of helium. The electric field $\mathbf{E}(t) = -\dot{\mathbf{A}}(t)$ of the OTC pulse with components E_x, E_y follows from

$$\mathbf{A}(t) = -\frac{E_0}{\omega} f(t)\left(\sin(\omega t)\hat{\mathbf{e}}_x + \frac{\epsilon}{n}\sin(n\omega t + \phi)\hat{\mathbf{e}}_y\right), \tag{2}$$

with unit vectors $\hat{\mathbf{e}}_x$ and $\hat{\mathbf{e}}_y$. Here, E_0 and $\omega = 2\pi/T$ are the peak field strength and the frequency of the fundamental laser pulse. The simulations are carried out for two fundamental laser wavelengths, namely 800 nm (with intensity 4.0×10^{14} W/cm^2) and 1200 nm (with intensity 3.51×10^{14} W/cm^2). The two-color delay ϕ quantifies the phase relation between the streaking field with frequency $n\omega$ and the fundamental field, and the relative amplitude is $\epsilon = 0.02$. In the TDSE simulations, the envelope $f(t)$ covers the range $[-T, 2T]$ and it consists of one-cycle edges and a one-cycle flat top. To suppress HHG contributions from the edges, they are chosen as $[\cos(\omega t/4)]^6$ for the leading edge and symmetrically for the trailing edge. This very short envelope allows us to consider not only integer, but arbitrary $n > 0$, while an experimental realization will probably use multicycle pulses and integer n. In each time step, the wave function is multiplied with a $\cos^{1/8}$-shaped mask to avoid reflections from the boundary. The masks start at $|x| = 1.1E_0/\omega^2$ for the x direction and at $|y| = 40$ a.u. for the y direction.

From the TDSE wave function, the dipole acceleration $\mathbf{a}(t) = -\partial_t^2\langle\mathbf{r}\rangle$ with components $a_x(t)$ and $a_y(t)$ is computed via the Ehrenfest theorem. In general, more than one trajectory contributes to the generation of one harmonic order [14,15,29], i.e., there are several pairs of ionization and recombination times. In particular, in each optical cycle there is a short and a long trajectory. Experimentally, the short trajectory can be selected by macroscopic phase matching [30]. To select a single short trajectory in the flat-top part of the pulse from the TDSE calculations, we resort to the Gabor time-frequency distribution [17,31]

$$\begin{aligned} I_{\mathrm{G}}(\Omega, t) &= I_{\mathrm{G}x}(\Omega, t) + I_{\mathrm{G}y}(\Omega, t) \\ &= \sum_{j=x,y}\left|\int dt' a_j(t') e^{-(t'-t)^2/(2\sigma^2)+i\Omega t'}\right|^2, \end{aligned} \tag{3}$$

with $\sigma = 1/(3\omega)$. Here, the total signal $I_{\mathrm{G}}(\Omega, t)$ is the sum of the intensities polarized along the x and y axes. For a given harmonic frequency Ω, the local maximum of the time-dependent Gabor intensity corresponding to the short trajectory is found at an emission time t_e, which depends on Ω and lies between $0.3\,T$ and $0.7\,T$. The value of I_{G} at the time t_e is used as the frequency-dependent harmonic signal for the further analysis. In this spirit, the two crucial ϕ-dependent observables within the streaking scheme are the harmonic intensity $I_G(\Omega, t_e)$ and the amplitude ratio R of the components polarized along y and x, $R(\Omega) = \sqrt{I_{Gy}(\Omega, t_e)/I_{Gx}(\Omega, t_e)}$. These two observables were previously used to deduce the ionization time t_i and recombination time t_r for each harmonic order [16,17]. The idea is that the two times are dictated by the fundamental field only, since the probe field is weak, but the two observables depend on the probe field as follows. HHG is possible only if the transverse displacement of the electron between ionization and recollision is zero, so that the returning electron hits the parent ion, i.e., $y(t_r) - y(t_i) = 0$, where $y(t)$ is the transverse electron coordinate. To satisfy this condition for a Coulomb-free Newtonian trajectory, it is necessary that the initial lateral velocity of the electron is

$$v_{y0} = -\frac{\epsilon E_0}{n\omega}\left[\sin(\varphi_i) + \frac{\cos(\varphi_r) - \cos(\varphi_i)}{n\omega(t_r - t_i)}\right], \tag{4}$$

where we define $\varphi_i = n\omega t_i + \phi$ and $\varphi_r = n\omega t_r + \phi$. It is known [32,33] that ionization and thus HHG is strongest for zero initial lateral velocity. Since we use complex-time trajectories, this condition reads [17,34]

$$\mathrm{Re}\, v_{y0} = 0. \tag{5}$$

Hence Eqs. (4) and (5) quantify how the optimal phase $\bar{\phi}$ that maximizes the harmonic signal is related to the complex ionization and recombination times. For linearly polarized harmonics and initial states with spherical symmetry, the y-to-x amplitude ratio R is related to the polarization angle of the harmonics relative to the x direction and hence to the return angle of the electron. In the experiment [16], R was measured by the amplitude ratio of the adjacent even and odd harmonics because, in an ω–2ω OTC field, even harmonics are polarized along y and odd harmonics are polarized along x. In analogy to Eq. (4), the trajectory model can be used to express R in terms of t_i, t_r, φ; see Refs. [16,17] for details. From those works, it is known that the probe-induced variation of the harmonic intensity depends predominantly on the ionization time, while the variation of the amplitude ratio depends predominantly on the return time.

Figure 1 shows the harmonic intensity (left column) and the amplitude ratio (right column) from the numerical solution of the TDSE as functions of harmonic order and two-color delay for ω–2ω (upper row) and ω–4.3ω (bottom row) fields. For each harmonic order, we find the optimal phases that maximize the observables, shown as orange dashed-dotted lines. For comparison, the white lines represent the optimal phases obtained from a simple implementation of the SFA: the harmonic intensity is $I_s(\Omega) = |\exp[i(\Omega t_r - S_v)]|^2$ with the action $S_v = \int_{t_i}^{t_r} dt[\mathbf{v}^2(t)/2 + I_p]$. Here, the velocity $\mathbf{v}$ with components v_x, v_y takes the form $\mathbf{v}(t) = \mathbf{p}(t_i, t_r) + \mathbf{A}(t)$ and the saddle-point momentum is $\mathbf{p}(t_i, t_r) = -1/(t_r - t_i)\int_{t_i}^{t_r}\mathbf{A}(t)dt$.

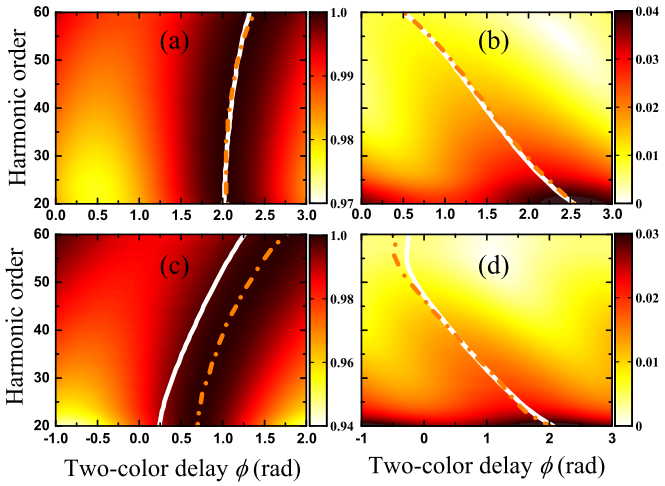

FIG. 1. Color density plots showing results from the numerical solution of the TDSE as a function of harmonic order and two-color delay: (a),(c) normalized harmonic signal and (b),(d) y-to-x amplitude ratio R of harmonics. The streaking frequency is 2ω (4.3ω) in the upper (lower) panels, where ω refers to the fundamental 800 nm pulse. The optimal phases maximizing the observables are shown by white solid curves (SFA) and orange dashed-dotted curves (TDSE).

The complex times $t_i = t_i^0 + i\,\mathrm{Im}t_i$ and $t_r = t_r^0 + i\,\mathrm{Im}t_r$ are solutions of the saddle-point equations of the QO model [15] (neglecting the field in y direction)

$$v_x^2(t_i)/2 = -I_p, \quad v_x^2(t_r)/2 = \Omega - I_p. \tag{6}$$

In the ω–2ω case, the optimal phases of TDSE agree excellently with the SFA model [see Figs. 1(a) and 1(b)], despite the lack of Coulomb effects in the SFA model and in agreement with earlier research results [17]. In the ω–4.3ω case, the optimal phases for the amplitude ratio are still very similar in TDSE and SFA [Fig. 1(d)]. However, a distinct shift appears in the optimal phases for the harmonic yield [Fig. 1(c)]. Does this phase shift reflect the Coulomb-induced ionization-time shift? We unveil the physics behind this phenomenon next.

To simplify the analysis, we make two assumptions. First, we perform the ionization-time retrieval from the harmonic yield only, while assuming that the return time is given by the QO model. We have numerically confirmed that this assumption has negligible effect on the resulting ionization times. This is consistent with (i) the finding of the analytical R-matrix (ARM) method [26] that the return time is less affected by the Coulomb potential than the ionization time, (ii) the observation that Coulomb focusing plays an insignificant role in the polarization angle for short trajectories [35], and (iii) the small deviation of the amplitude ratio from the QO model in Figs. 1(b) and 1(d). The imaginary part of the return time is small and it is neglected [17,36]. Second, we assume that the imaginary part of t_i equals the Keldysh tunneling time, $\mathrm{Im}t_i = \sqrt{2I_p}/|E_x(t_i^0)|$ [37]. Thus the real part t_i^0 is retrieved via Eqs. (4) and (5) in combination with the optimal phases obtained for the harmonic intensity from the numerical solution of the TDSE.

The results obtained for various streaking frequencies $n\omega$ are shown in Fig. 2(a). In the low-frequency domain ($n \leqslant 2$), the retrieved times agree with the QO times, which do not include Coulomb effects. In the high-frequency domain ($n \geqslant 3$), there is a shift to earlier times.

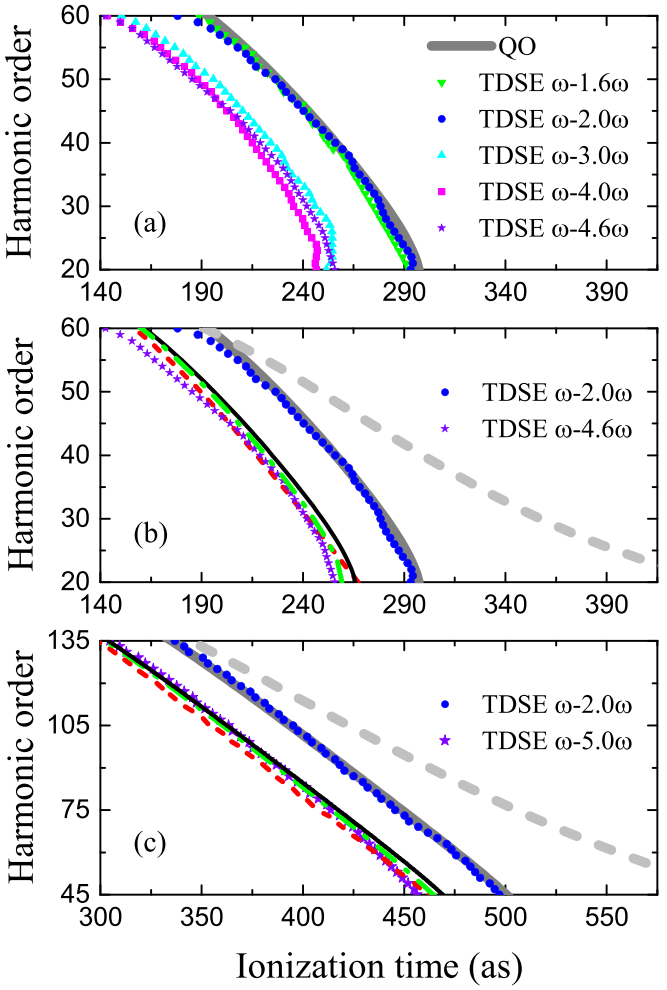

FIG. 2. (a) Ionization times retrieved from TDSE with various streaking frequencies for 800 nm. (b),(c) Representative TDSE results for low-frequency and high-frequency streaking using fundamental wavelengths (b) 800 nm and (c) 1200 nm, together with ionization times from the adiabatic correction (black line), CM (red dashed line), ARM theory (green dashed-dotted line), and simple man's model, i.e., QO model with $I_p = 0$ (thick dashed light-gray line). Thick solid gray lines in (a),(b),(c) show the real parts of the QO model times. The field intensities are (a),(b) 4.0×10^{14} W/cm^2 and (c) 3.51×10^{14} W/cm^2.

To interpret these results, we calculate the Coulomb-corrected ionization time in the absence of the probe field using three different models. (i) Adiabatic correction: immediately after ionization, the attractive Coulomb force slows down the outgoing electron. Approximating the ionizing field $E_x(t_i^0)$ as static, the resulting velocity change is $v_0^e = \pi E_x(t_i^0)/(2I_p)^{3/2}$ [38]. To produce the same return energy as without the Coulomb potential, the electron must be released earlier to receive more laser-induced acceleration, changing the ionization time (relative to the QO time) by

$$\delta t_i^0 = -\frac{\pi}{(2I_p)^{3/2}}. \tag{7}$$

(ii) Classical model (CM): the electron trajectory $\mathbf{r}(t)$ is dictated by Newton's equation $\ddot{\mathbf{r}}(t) = -\mathbf{E}(t) - \partial_{\mathbf{r}} V(\mathbf{r}(t))$ with

initial conditions based on the SFA, i.e., $\dot{\mathbf{r}}(t_i^0) = \mathrm{Re}[\mathbf{p}(t_i, t_r) + \mathbf{A}(t_i^0)]$ and $\mathbf{r}(t_i^0) = \mathrm{Re}(\int_{t_i}^{t_i^0}[\mathbf{p}(t_i, t_r) + \mathbf{A}(t)]dt)$. The classical recombination time t_r' corresponding to these initial conditions is defined by $\mathbf{r}(t_r') = 0$. The total (kinetic and potential) energy of the electron at t_r' determines the radiated photon energy

$$\Omega'\left(t_i^0, t_r'\right) = I_p + \dot{\mathbf{r}}^2(t_r')/2 + V(\mathbf{r}(t_r')). \tag{8}$$

This provides the desired mapping from harmonic frequencies Ω' to ionization times t_i^0. (iii) ARM [26,39,40]: a Coulomb term S_c is added to the SFA action to treat the first-order effect of the electron-core interaction $U_c(\mathbf{r}) = -1/\sqrt{\mathbf{r}^2}$ in HHG. In detail,

$$S_c = \int_{t_k}^{t_f} dt\, U(\mathbf{r}_a(t)), \tag{9}$$

where $\mathbf{r}_a(t) = \int_{t_i}^{t}[\mathbf{p}(t_i, t_r)+\mathbf{A}(t')]dt'$ is the potential-free trajectory. The lower integration limit is $t_k = t_i - i/(2I_p)$ and the upper limit t_f is determined by the return condition $\sqrt{\mathbf{r}_a(t_f)^2} = \exp[2(0.5772 - \xi)]/(2v_r)$ with $\xi = \sum_{p=1}^{\infty}\{1 - v_r\, p \arctan[1/(v_r\, p)]\}/p$ and the return velocity $v_r = \sqrt{2(\Omega - I_p)}$. Expanding the saddle-point times yields the first-order time shifts [26]

$$\Delta t_i^0 = -\frac{\partial\, \mathrm{Re}S_c}{\partial I_p} - \frac{\partial\, \mathrm{Re}S_c}{\partial \Omega}, \quad \Delta t_r^0 = -\frac{\partial\, \mathrm{Re}S_c}{\partial \Omega}. \tag{10}$$

The integration contour in Eq. (9) is chosen as $t_k \to \mathrm{Re}\, t_k \to \mathrm{Re}\, t_f \to t_f$, which does not cross branch cuts [26,41]. In practice, Δt_i^0 and Δt_r^0 are found by calculating S_c for closely lying values of I_p and Ω.

The Coulomb-corrected ionization times are shown in Fig. 2(b) for the wavelength 800 nm at the intensity 4.0×10^{14} W/cm^2. Similar results are obtained for the wavelength 1200 nm at the intensity 3.51×10^{14} W/cm^2; see Fig. 2(c). The adiabatic correction, CM, and ARM theory agree well with each other and they exhibit an amazing consistency with the times retrieved from the TDSE two-color scheme with high streaking frequency. Apparently, the Coulomb shifts can be accurately measured by an appropriate choice of the streaking frequency. We also note that the good performance of the adiabatic correction, Eq. (7), suggests that the physical picture of a Coulomb-induced slowdown after ionization is adequate.

To consolidate the physical picture, we extend the CM and ARM methods to the full OTC field. Here, the aim is to set up approximate theories as an alternative to TDSE to obtain optimal phases from which the ionization time can be retrieved. In the CM, the optimal phase $\bar{\phi}$ is defined such that the transverse trajectory returns to zero at t_r', i.e., $y(t_r') = 0$. To satisfy Eq. (5), the lateral initial condition $\dot{y}(t_i^0) = \mathrm{Re}[A_y(t_i^0) - A_y(t_i)]$ is used. Here, A_y is the y component of $\mathbf{A}$. In ARM, the optimal phase is found by maximizing the harmonic intensity

$$I_a = |\exp[i\Omega t_r'' - iS_v(t_i'', t_r'') - iS_c(t_i'', t_r'')]|^2. \tag{11}$$

Here, the saddle-point times t_i'', t_r'' for the OTC field (not just the fundamental field) are used because of the sensitivity of the Coulomb term to the times. From the optimal phase of CM and ARM, we retrieve the ionization times using the same procedure as from the TDSE optimal phase. For the fundamental wavelength 800 nm, Fig. 3 shows these times as a function of the streaking frequency $n\omega$ for two harmonic orders. Even though TDSE, CM, and ARM differ in the details, we find that they all produce a double-plateau structure with a smooth transition from the low-frequency to the high-frequency regime. In the first plateau, the retrieved ionization time agrees with the QO time, as if no Coulomb interaction was present. This is reminiscent of the absence of a Coulomb shift when orthogonal streaking was applied to the bicircular attoclock [42], where high effective probe frequencies were not studied. The second plateau, however, matches the Coulomb-corrected times.

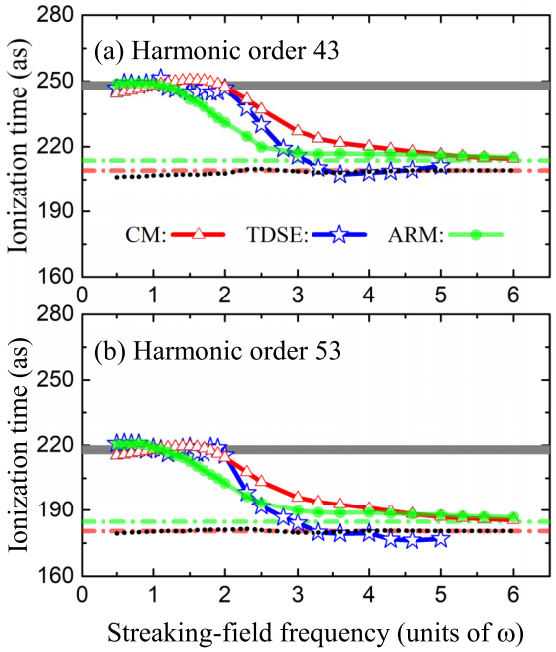

FIG. 3. Retrieved ionization times versus streaking frequency for harmonic orders (a) 43 and (b) 53 in HHG with the fundamental wavelength 800 nm. The horizontal lines show reference times without streaking: QO (gray solid lines), CM (red dashed-dotted lines), and ARM (green dashed-dotted lines). Black dotted lines show the two-color CM without lateral Coulomb force.

In a modified CM where we neglect the Coulomb force along the y axis, the retrieved ionization time is almost independent of the streaking frequency and it agrees with the TDSE high-frequency plateau (see the dotted line in Fig. 3), indicating that Coulomb effects in the probe direction are responsible for the error of the OTC method at low frequency.

Our work is relevant for experiment as it indicates that short probe wavelengths such as 200 nm (corresponding to 4ω for an 800 nm fundamental field) are superior in measuring times with attosecond precision. For none of the investigated fundamental wavelengths is the probe wavelength 400 nm short enough for precisely measuring the ionization time via the Coulomb-free scheme. We have found that these conclusions are independent of the probe field strength as long as $\epsilon \lesssim 0.1$. We believe that the transition frequency between the low- and high-frequency streaking regimes is related to the Keldysh time $\tau_K = \sqrt{2I_p}/|E_x|$ of the ionizing field because the Coulomb-free Eq. (4) acquires large values due to the

imaginary part of $n\omega t_i$ in the regime $n\omega\tau_K \gg 1$ so that it can dominate over Coulomb effects. We have numerically confirmed that, for high streaking frequency, including an approximate Coulomb term in Eq. (4) causes negligible changes.

To our knowledge, 800 nm–200 nm OTC HHG, which has the additional benefit of y-polarized even harmonics (as in the ω–2ω case), has not been implemented yet. But other nonstandard probe wavelengths have already attracted attention [43–45], showing the feasibility of streaking at various wavelengths. The absolute two-color delay is usually unknown in experiment. To this end, the y-to-x amplitude ratio provides a useful gauge for the two-color delay as it is well predicted by SFA theory; see Figs. 1(b) and 1(d).

In summary, we have investigated the frequency dependence of two-color HHG for the measurement of ionization times on the attosecond time scale. Our results indicate that high streaking frequencies are well suited for resolving tiny time shifts caused by the electron-core interaction. In the future, this approach can facilitate the attosecond-scale investigation of orientation-dependent strong-field ionization of molecules.

We thank N. Eicke, X. Zhu, and S. Brennecke for valuable discussions. We thank O. Smirnova and L. Torlina for providing the imaginary parts of the ARM Coulomb time shifts as a cross-check for our calculation. This work has been supported by the China Scholarship Council, the Deutsche Forschungsgemeinschaft through the Priority Programme 1840, and by the National Natural Science Foundation of China (Grants No. 11874030 and No. 11904146).

[1] S. Grundmann, D. Trabert, K. Fehre, N. Strenger, A. Pier, L. Kaiser, M. Kircher, M. Weller, S. Eckart, L. P. H. Schmidt, F. Trinter, T. Jahnke, M. S. Schöffler, and R. Dörner, Zeptosecond birth time delay in molecular photoionization, Science **370**, 339 (2020).

[2] T. Gaumnitz, A. Jain, Y. Pertot, M. Huppert, I. Jordan, F. Ardana-Lamas, and H. J. Wörner, Streaking of 43-attosecond soft-X-ray pulses generated by a passively cep-stable mid-infrared driver, Opt. Express **25**, 27506 (2017).

[3] J. Li, X. Ren, Y. Yin, K. Zhao, A. Chew, Y. Cheng, E. Cunningham, Y. Wang, S. Hu, Y. Wu, M. Chini, and Z. Chang, 53-attosecond X-ray pulses reach the carbon K-edge, Nat. Commun. **8**, 186 (2017).

[4] S. Koke, C. Grebing, H. Frei, A. Anderson, A. Assion, and G. Steinmeyer, Direct frequency comb synthesis with arbitrary offset and shot-noise-limited phase noise, Nat. Photon. **4**, 462 (2010).

[5] J. Köhler, M. Wollenhaupt, T. Bayer, C. Sarpe, and T. Baumert, Zeptosecond precision pulse shaping, Opt. Express **19**, 11638 (2011).

[6] J. Itatani, F. Quéré, G. L. Yudin, M. Y. Ivanov, F. Krausz, and P. B. Corkum, Attosecond Streak Camera, Phys. Rev. Lett. **88**, 173903 (2002).

[7] P. M. Paul, E. S. Toma, P. Breger, G. Mullot, F. Augé, P. Balcou, H. G. Muller, and P. Agostini, Observation of a train of attosecond pulses from high harmonic generation, Science **292**, 1689 (2001).

[8] H. G. Muller, Reconstruction of attosecond harmonic beating by interference of two-photon transitions, Appl. Phys. B **74**, s17 (2002).

[9] P. Eckle, M. Smolarski, P. Schlup, J. Biegert, A. Staudte, M. Schöffler, H. G. Muller, R. Dörner, and U. Keller, Attosecond angular streaking, Nat. Phys. **4**, 565 (2008).

[10] U. S. Sainadh, H. Xu, X. Wang, A. Atia-Tul-Noor, W. C. Wallace, N. Douguet, A. Bray, I. Ivanov, K. Bartschat, A. Kheifets, R. T. Sang, and I. V. Litvinyuk, Attosecond angular streaking and tunnelling time in atomic hydrogen, Nature (London) **568**, 75 (2019).

[11] N. Eicke and M. Lein, Attoclock with counter-rotating bicircular laser fields, Phys. Rev. A **99**, 031402(R) (2019).

[12] P. B. Corkum, Plasma Perspective on Strong Field Multiphoton Ionization, Phys. Rev. Lett. **71**, 1994 (1993).

[13] K. C. Kulander, K. J. Schafer, and J. L. Krause, Dynamics of short-pulse excitation, ionization and harmonic conversion, in *Super-Intense Laser-Atom Physics*, edited by B. Pireaux, A. L'Huillier and K. Rzążewski, NATO ASI, Series B: Physics (Springer, Boston, 1993), Vol. 316.

[14] M. Lewenstein, P. Balcou, M. Y. Ivanov, A. L'Huillier, and P. B. Corkum, Theory of high-harmonic generation by low-frequency laser fields, Phys. Rev. A **49**, 2117 (1994).

[15] B. C. P. Salières, L. L. Déroff, F. Grasbon, G. G. Paulus, H. Walther, R. Kopold, W. Becker, D. B. Milošević, A. Sanpera, and M. Lewenstein, Feynman's path-integral approach for intense-laser-atom interactions, Science **292**, 902 (2001).

[16] D. Shafir, H. Soifer, B. D. Bruner, M. Dagan, Y. Mairesse, S. Patchkovskii, M. Y. Ivanov, O. Smirnova, and N. Dudovich, Resolving the time when an electron exits a tunnelling barrier, Nature (London) **485**, 343 (2012).

[17] J. Zhao and M. Lein, Determination of Ionization and Tunneling Times in High-Order Harmonic Generation, Phys. Rev. Lett. **111**, 043901 (2013).

[18] M. Kitzler and M. Lezius, Spatial Control of Recollision Wave Packets with Attosecond Precision, Phys. Rev. Lett. **95**, 253001 (2005).

[19] X. Xie, Two-Dimensional Attosecond Electron Wave-Packet Interferometry, Phys. Rev. Lett. **114**, 173003 (2015).

[20] M. Richter, M. Kunitski, M. Schöffler, T. Jahnke, L. P. H. Schmidt, M. Li, Y. Q. Liu, and R. Dörner, Streaking Temporal Double-Slit Interference by an Orthogonal Two-Color Laser Field, Phys. Rev. Lett. **114**, 143001 (2015).

[21] J. Henkel and M. Lein, Analysis of electron trajectories with two-color strong-field ionization, Phys. Rev. A **92**, 013422 (2015).

[22] X. Gong, C. Lin, F. He, Q. Song, K. Lin, Q. Ji, W. Zhang, J. Ma, P. Lu, Y. Liu, H. Zeng, W. Yang, and J. Wu, Energy-Resolved Ultrashort Delays of Photoelectron Emission Clocked by Orthogonal Two-Color Laser Fields, Phys. Rev. Lett. **118**, 143203 (2017).

[23] D. Würzler, N. Eicke, M. Möller, D. Seipt, A. M. Sayler, S. Fritzsche, M. Lein, and G. G. Paulus, Velocity map imaging of

scattering dynamics in orthogonal two-color fields, J. Phys. B: At. Mol. Opt. Phys. **51**, 015001 (2018).

[24] V. Tulsky and D. Bauer, QPROP with faster calculation of photoelectron spectra, Comput. Phys. Commun. **251**, 107098 (2020).

[25] L. Brugnera, D. J. Hoffmann, T. Siegel, F. Frank, A. Zaïr, J. W. G. Tisch, and J. P. Marangos, Trajectory Selection in High Harmonic Generation by Controlling the Phase between Orthogonal Two-Color Fields, Phys. Rev. Lett. **107**, 153902 (2011).

[26] L. Torlina and O. Smirnova, Coulomb time delays in high harmonic generation, New J. Phys. **19**, 023012 (2017).

[27] J. Crank and P. Nicolson, A practical method for numerical evaluation of solutions of partial differential equations of the heat-conduction type, Math. Proc. Cambr. Philos. Soc. **43**, 50 (1947).

[28] M. Nurhuda and F. H. M. Faisal, Numerical solution of time-dependent Schrödinger equation for multiphoton processes: A matrix iterative method, Phys. Rev. A **60**, 3125 (1999).

[29] A. Zaïr, M. Holler, A. Guandalini, F. Schapper, J. Biegert, L. Gallmann, U. Keller, A. S. Wyatt, A. Monmayrant, I. A. Walmsley, E. Cormier, T. Auguste, J. P. Caumes, and P. Salières, Quantum Path Interferences in High-Order Harmonic Generation, Phys. Rev. Lett. **100**, 143902 (2008).

[30] P. Balcou, P. Salières, A. L'Huillier, and M. Lewenstein, Generalized phase-matching conditions for high harmonics: The role of field-gradient forces, Phys. Rev. A **55**, 3204 (1997).

[31] C. C. Chirilă, I. Dreissigacker, E. V. van der Zwan, and M. Lein, Emission times in high-order harmonic generation, Phys. Rev. A **81**, 033412 (2010).

[32] F. Krausz and M. Ivanov, Attosecond physics, Rev. Mod. Phys. **81**, 163 (2009).

[33] M. Y. Ivanov, M. Spanner, and O. Smirnova, Anatomy of strong field ionization, J. Mod. Opt. **52**, 165 (2005).

[34] We have confirmed numerically that the optimal phase estimated by Re $v_{y0} = 0$ is consistent with that from the SFA model.

[35] D. Shafir, B. Fabre, J. Higuet, H. Soifer, M. Dagan, D. Descamps, E. Mével, S. Petit, H. J. Wörner, B. Pons, N. Dudovich, and Y. Mairesse, Role of the Ionic Potential in High Harmonic Generation, Phys. Rev. Lett. **108**, 203001 (2012).

[36] E. V. van der Zwan and M. Lein, Molecular Imaging Using High-Order Harmonic Generation and Above-Threshold Ionization, Phys. Rev. Lett. **108**, 043004 (2012).

[37] L. V. Keldysh, Ionization in the field of a strong electromagnetic wave, Sov. Phys. JETP **20**, 1307 (1965).

[38] N. I. Shvetsov-Shilovski, S. P. Goreslavski, S. V. Popruzhenko, and W. Becker, Capture into Rydberg states and momentum distributions of ionized electrons, Laser Phys. **19**, 1550 (2009).

[39] L. Torlina and O. Smirnova, Time-dependent analytical R-matrix approach for strong-field dynamics. I. One-electron systems, Phys. Rev. A **86**, 043408 (2012).

[40] M. Ivanov and O. Smirnova, How Accurate Is the Attosecond Streak Camera?, Phys. Rev. Lett. **107**, 213605 (2011).

[41] S. V. Popruzhenko, Coulomb phase in high harmonic generation, J. Phys. B: At. Mol. Opt. Phys. **51**, 144006 (2018).

[42] N. Eicke, S. Brennecke, and M. Lein, Attosecond-Scale Streaking Methods for Strong-Field Ionization by Tailored Fields, Phys. Rev. Lett. **124**, 043202 (2020).

[43] S. Watanabe, K. Kondo, Y. Nabekawa, A. Sagisaka, and Y. Kobayashi, Two-Color Phase Control in Tunneling Ionization and Harmonic Generation by a Strong Laser Field and Its Third Harmonic, Phys. Rev. Lett. **73**, 2692 (1994).

[44] T. Kroh, C. Jin, P. Krogen, P. D. Keathley, A. L. Calendron, J. P. Siqueira, H. K. Liang, E. L. Falcão-Filho, C. D. Lin, F. X. Kärtner, and K. H. Hong, Enhanced high-harmonic generation up to the soft X-ray region driven by mid-infrared pulses mixed with their third harmonic, Opt. Express **26**, 16955 (2018).

[45] S. Mitra, S. Biswas, J. Schötz, E. Pisanty, B. Förg, G. A. Kavuri, C. Burger, W. Okell, M. Högner, I. Pupeza, V. Pervak, M. Lewenstein, P. Wnuk, and M. F. Kling, Suppression of individual peaks in two-colour high harmonic generation, J. Phys. B: At. Mol. Opt. Phys. **53**, 134004 (2020).